44th AIAA Aerospace Sciences Meeting and Exhibit, 9-12 January 2006, Reno, Nevada

Prediction of the Flow Around a Circular Cylinder at High Reynolds Number

Vivek Krishnan* and Kyle D. Squires†

MAE Department, Arizona State University, Tempe, AZ 85287-6106, USA

James R. Forsythe‡

Cobalt Solutions LLC, 4636 New Carlisle Pike, Springfield, OH 45504-3336, USA

Detached-Eddy Simulation (DES) is applied to prediction of the super-critical flow around a circular cylinder. One of the primary aims is to assess a new DES version developed by Spalart *et al.*[1] against results obtained using the baseline method. In the new version of the technique, known as Delayed Detached Eddy Simulation (DDES), the turbulent length scale is determined using information from the eddy viscosity field, in addition to the wall distance and grid spacing. Computations are performed at Reynolds numbers, Re, based on the freestream velocity and cylinder diameter of 1.4×10^5 and 8×10^6, with the lower Re predictions assessed against previous simulations and the higher Re assessed against experimental measurements. Flow visualizations show that there is comparable eddy content resolved using the baseline and new DES versions. At $Re = 1.4 \times 10^5$, predictions of the drag coefficient, separation angle, and pressure distribution are in good agreement with the fully turbulent solutions of Travin *et al.*[2] and Hansen and Forsythe.[3] Predictions at $Re = 8 \times 10^6$ are obtained using three grids with the coarsest mesh having 1.47×10^6 cells and the finest grid having 9.83×10^6 cells. The force histories and averaged force coefficients obtained using both models are in good agreement. Predictions of the pressure coefficient using the baseline and new DES versions are in the range of experimental measurements.

I. Introduction

Detached-Eddy Simulation was proposed by Spalart *et al.*[4] as a numerically feasible and plausibly accurate approach for prediction of massively separated flows at high Reynolds numbers. Traditionally, even massively separated flows have been modeled using Reynolds-averaged Navier-Stokes (RANS) methods. The performance of RANS models in predicting this class of flows is, at best, uneven with definitive failures in configurations as basic as a flat plate at incidence, among other issues. Large-Eddy Simulation is much less sensitive to turbulence modeling errors since only the small, subgrid scales of motion are modeled, but the computational cost of resolving turbulent boundary layers limits LES to moderate Reynolds numbers.

Since its inception, there have been substantial efforts in application and assessment of DES. An array of flows ranging from "building block" applications such as the flow over a cylinder, sphere, aircraft forebody, and missile base to complex geometries including full aircraft have been modeled,[2,5,6,7,3,8,9,10,11] These and other applications have been largely successful, illustrating DES capabilities in accurately resolving chaotic unsteady features in the separated regions along with a rational treatment of the attached boundary layers.

The solution field in a DES is comprised of its "RANS Region" in which a RANS turbulence model is active and an "LES Region" in which an LES treatment is applied. In natural DES applications, such as the examples cited above, the "RANS Region" constitutes the entire boundary layer and with the "LES

*Research Assistant.

†Professor, AIAA Member.

‡Director of Research, and Senior Member AIAA.

Region" comprising the separated regions. The original version of the method, which is referred to as DES97 throughout this manuscript, is based on the Spalart-Allmaras[12] eddy viscosity model and achieves LES behavior by modifying the length scale that enters the turbulence model. This length scale, $\widetilde{d}$, is defined as the minimum of the distance to the nearest wall, d, and a length scale proportional to the local grid spacing, i.e., $\widetilde{d} = \min(d, C_{DES}\Delta)$ where typically $C_{DES} = 0.65$ and $\Delta = \max(\Delta_x, \Delta_y, \Delta_z)$. Sensitizing the length scale to the mesh yields a Smagorinsky-like eddy viscosity in the LES region that is lower than would be the corresponding RANS viscosity and, consequently, lowers the modeled stresses in the LES region. Mesh resolutions in the LES region must then be sufficiently fine to support resolved stresses derived from velocity fluctuations supported on the grid.

For natural DES applications with RANS-type grids in the boundary layers the wall-parallel grid spacings determine Δ and are typically comparable to or larger than the boundary layer thickness. Thus, the length scale $\widetilde{d}$ within the boundary layer takes its RANS value, d. As described in Spalart *et al.*,[1] scenarios are also possible in which the length scale $\widetilde{d}$ may not maintain its RANS value $\widetilde{d} = d$ throughout the boundary layer. For example, in applications that focus on wall-modeling for LES, $\widetilde{d} = C_{DES}\Delta$ is purposefully desired within the boundary layer because relatively fine grid resolutions are used that support resolved velocity fluctuations. In other regimes, however, boundary layer grids might be characterized by mesh spacings that result in the LES value for the length scale ($\widetilde{d} = C_{DES}\Delta$) well inside the boundary layer but without sufficient resolution to sustain velocity fluctuations on the grid. This can occur through grid refinement which will decrease the wall-parallel grid spacings for a given boundary layer thickness δ or a thickening boundary layer that can effectively reduce the wall-parallel spacings relative to δ. This regime is undesirable in applications because turbulent stresses (both resolved and modeled) will be too low and prediction of quantities such as the skin friction will be degraded.

Spalart *et al.*[1] refer to this effect as "Modeled Stress Depletion" and proposed a new version of the technique that addresses this issue. The new version is referred to as Delayed Detached-Eddy Simulation (DDES) and addresses natural applications where it is desired to maintain RANS behavior throughout the boundary layer, irrespective of the grid spacings. As described in their work,[1] DDES is based on a simple modification to DES97 and is similar to the proposal of Menter and Kuntz[13] developed for the SST model. Assessment of DDES reported by Spalart *et al.*[1] was favorable and motivated the current application to the super-critical flow around a circular cylinder.

The cylinder flow is a challenging test case for any turbulence simulation strategy and the main goal of the present effort is to assess the new DES model. Computations are performed at a Reynolds number $Re = 1.4 \times 10^5$ for which DES predictions obtained by Travin *et al.*[2] and Hansen and Forsythe[3] are available for assessment of the simulations performed in this study. Mesh refinement is investigated at a higher Reynolds number, $Re = 8 \times 10^6$, where experimental measurements obtained by Roshko[14] and van Nunen[15] provide a means for assessing the calculations.

Presented in the following sections is an overview of the turbulence models followed by a description of the simulation parameters and cases. Results at the lower Reynolds number are then presented followed by the predictions at the higher Reynolds number. Finally, a summary and perspectives on the work are also presented.

II. Detached-Eddy Simulation

A. Spalart-Allmaras Model

The baseline version DES97 is formulated using the Spalart-Allmaras (referred to as 'S-A' throughout) one-equation model,[12] which solves solves a single partial differential equation for a variable $\widetilde{\nu}$ which is related to the turbulent viscosity. The model includes a wall destruction term that reduces the turbulent viscosity in the log layer and laminar sublayer and trip terms that provides a smooth transition from laminar to turbulent flow. In the present computations of the super-critical flow, the trip terms are not included and the model then takes the form,

$$\frac{D\widetilde{\nu}}{Dt} = c_{b1}\widetilde{S}\,\widetilde{\nu} - c_{w1}f_w\left[\frac{\widetilde{\nu}}{d}\right]^2 + \frac{1}{\sigma}\left[\nabla\cdot\left(\left(\nu+\widetilde{\nu}\right)\nabla\widetilde{\nu}\right) + c_{b2}\left(\nabla\widetilde{\nu}\right)^2\right]. \quad (1)$$

The turbulent viscosity is determined via,

$$\nu_t = \widetilde{\nu}\, f_{v1}, \qquad f_{v1} = \frac{\chi^3}{\chi^3 + c_{v1}^3}, \qquad \chi \equiv \frac{\widetilde{\nu}}{\nu}\,, \tag{2}$$

where ν is the molecular viscosity. Using S to denote the magnitude of the vorticity, the modified vorticity $\widetilde{S}$ is defined as,

$$\widetilde{S} \equiv S + \frac{\widetilde{\nu}}{\kappa^2 d^2} f_{v2}\,, \qquad f_{v2} = 1 - \frac{\chi}{1 + \chi f_{v1}}\,, \tag{3}$$

where d is the distance to the closest wall. The wall destruction function, f_w is,

$$f_w = g\left[\frac{1 + c_{w3}^6}{g^6 + c_{w3}^6}\right]^{\frac{1}{6}}, \qquad g = r + c_{w2}(r^6 - r)\,, \qquad r \equiv \frac{\widetilde{\nu}}{\widetilde{S}\kappa^2 d^2}\,. \tag{4}$$

The closure coefficients are given by:

$$\begin{array}{ccc} c_{b1} = 0.1355 & \sigma = 2/3 & c_{b2} = 0.622 \\ \kappa = 0.41 & c_{w1} = c_{b1}/\kappa^2 + (1 + c_{b2})/\sigma & c_{w2} = 0.3 \\ c_{w3} = 2 & c_{v1} = 7.1 & \end{array} \tag{5}$$

B. Detached-Eddy Simulation

1. Baseline Version – DES97

The baseline formulation, DES97, is a modification of the Spalart-Allmaras RANS model (1) such that the model reduces to its RANS formulation near solid surfaces and to a subgrid model away from the wall. As described above, the DES formulation is obtained by replacing in the S-A model the distance to the nearest wall, d, by $\widetilde{d}$, where $\widetilde{d} \equiv \min(d, C_{DES}\Delta)$. For the unstructured grids used in the present computations the lengthscale Δ is taken as the largest distance between the cell center under consideration and the cell center of the neighbors (i.e., those cells sharing a face with the cell in question). The constant $C_{DES} = 0.65$ was set in homogeneous turbulence[16] and is used without modification in this study.

2. New Version – DDES

The new version of the model, Delayed Detached Eddy Simulation (DDES), modifies the length scale $\widetilde{d}$ in order to preserve RANS treatment of the boundary layer. As discussed in Spalart *et al.*,[1] the modification is analogous to that developed by Menter and Kuntz[13] which uses the blending function F_2 of the SST model. The essence of the modification is to utilize information concerning the lengthscale of the turbulence as predicted by the model, in addition to the wall distance and local grid spacing. The summary of the model as outlined below is taken from Spalart *et al.*[1] and the reader is referred to their work for a more complete presentation.

In DDES, the parameter r_d is introduced,

$$r_d \equiv \frac{\nu_t + \nu}{\sqrt{U_{i,j}U_{i,j}}\kappa^2 d^2}, \tag{6}$$

where $U_{i,j}$ are the velocity gradients. Similar to r in the S-A model, this parameter equals 1 in a logarithmic layer, and falls to 0 gradually towards the edge of the boundary layer. The addition of ν in the numerator corrects the very-near-wall behavior by ensuring that r_d remains away from 0. The quantity r_d is used as an argument to the function,

$$f_d \equiv 1 - \tanh([8r_d]^3)\,, \tag{7}$$

which is designed to be 1 in the LES region, where $r_d \ll 1$, and 0 elsewhere (and to be insensitive to r_d exceeding 1 very near the wall). The values 8 and 3 for the constants are based on shape requirements for f_d, and on tests of DDES in the flat-plate boundary layer. The DES length scale $\widetilde{d}$ is then re-defined as,

$$\widetilde{d} \equiv d - f_d \max(0, d - C_{DES}\Delta)\,. \tag{8}$$

Setting f_d to 0 yields RANS ($\widetilde{d} = d$), while setting it to 1 gives DES97. As noted in Spalart *et al.*,[1] for DES based on most of the possible RANS models, DDES will consist in multiplying by f_d the term that constitutes the difference between RANS and DES.

III. Simulation Overview

The solutions presented in this work are of the compressible Navier-Stokes equations on unstructured grids and obtained using *Cobalt*.[17] The numerical method is a cell-centered finite volume approach applicable to arbitrary cell topologies (e.g, hexahedron, prisms, tetrahedron). The spatial operator uses the exact Riemann solver of Gottlieb and Groth,[18] least squares gradient calculations using QR factorization to provide second order accuracy in space, and TVD flux limiters to limit extremes at cell faces. A point implicit method using analytical first-order inviscid and viscous Jacobians is used for advancement of the discretized system. For time-accurate computations, a Newton sub-iteration scheme is employed, the method is second order accurate in time. The domain decomposition library ParMETIS[19] is used for parallel implementation and communication between processors is achieved using Message Passing Interface.

Computations are performed at two Reynolds numbers (based on the freestream velocity and cylinder diameter D): 1.4×10^5 and 8×10^6. The spanwise coordinate of the domain along which periodic boundary conditions are applied is $4D$ for both Reynolds numbers. The calculations at $Re = 1.4 \times 10^5$ were performed using a mesh comprised of 1.434×10^6 cells, the same grid as used by Hansen and Forsythe[3] and characterized by a spanwise grid spacing $\Delta_z/D = 0.10$. The calculations at $Re = 1.4 \times 10^5$ were used to provide an initial assessment of the models against other DES results. The influence of mesh refinement is investigated at the higher Reynolds number using three grids having 1.46×10^6, 3.71×10^6, and 9.83×10^6 cells and are referred to as "coarse grid" or "cg", "medium grid" or "mg", and "fine grid" or "fg" below. Stretching was applied such that the spacing along the spanwise axis was up to 7.5 times larger than in the plane normal to the span in order to maintain feasible cell counts while still adequately resolving vortex shedding. The medium grid was created by refining in all directions the coarse by a factor of $\sqrt{2}$. The finer grid is another factor of $\sqrt{2}$ refinement in each coordinate direction. The corresponding spanwise grid spacings, which determine Δ in DES97, are $\Delta_z/D = 0.10$, $\Delta_z/D = 0.07$, and $\Delta_z/D = 0.05$ for the coarse, medium, and fine grids, respectively.

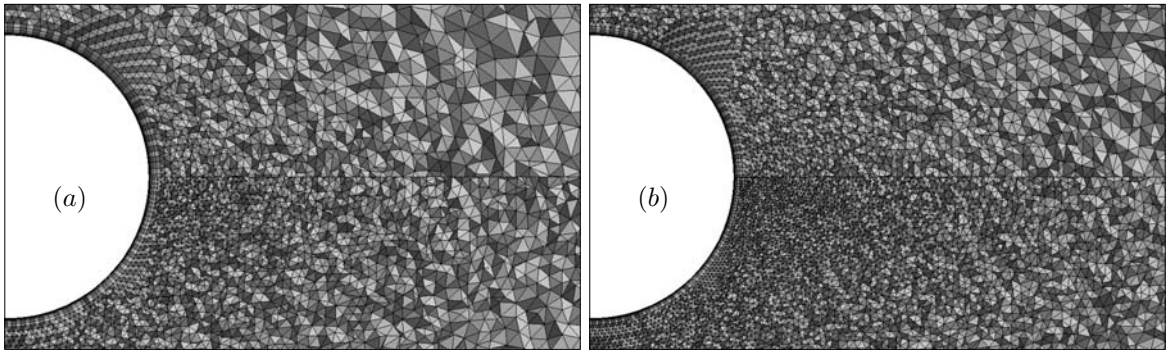

Figure 1. Cross-section of the grids in the vicinity of the cylinder. (a) coarse (upper half plane) and medium (lower half plane) grids; (b) medium (upper half plane) and fine (lower half plane).

Cross-sections of the mesh in the vicinity of the cylinder are shown in Figure 1. The grid was created using VGRIDns[20] and is comprised of prisms near the cylinder surface and tetrahedra away from the wall. For all of the grids the spacing from the cylinder surface, on which no-slip conditions are applied, to the cell center nearest the wall was within one viscous unit on average. A geometric stretching rate of 1.2 was applied to the wall-normal grid spacing within the boundary layer. Farfield conditions are applied at the outer boundaries of the computational domain that lie in the plane of the freestream velocity vector. The outer boundaries are located 20 diameters from the cylinder surface.

For both Reynolds numbers the super-critical flow is approximated by computing fully-turbulent solutions. At the inlet to the computational domain a small level of eddy viscosity (corresponding to $\chi = 3$) is prescribed that is sufficient to ignite the turbulence model as the fluid enters the boundary layers. For all of the simulations reported in this contribution the time step was fixed at $0.01D/U_\infty$ where U_∞ is the freestream velocity.

IV. Results

A. DES Predictions at $Re = 1.4 \times 10^5$

	C_d	$C_{l,rms}$	St	$-C_{pb}$	θ_{sep}
DES97	0.58	0.08	0.29	0.64	98°
DDES	0.60	0.11	0.28	0.69	99°
Travin *et al.*[2]	0.57	0.08	0.30	0.65	99°
Hansen *et al.*[3]	0.59	–	0.29	0.72	–
Roshko[14]	0.62-0.74	–	0.27	–	–

Table 1. Summary of $Re = 1.4 \times 10^5$ predictions.

Shown in Table 1 are averaged quantities from the current DES97 and DDES predictions of the flow at $Re = 1.4 \times 10^5$: the drag coefficient C_d, rms lift coefficient $C_{l,rms}$, shedding Strouhal number St, base pressure coefficient C_{pb}, and separation angle θ_{sep}. Also included are the DES97 predictions of Travin *et al.*[2] and Hansen and Forsythe[3] along with the experimental measurements reported in Roshko.[14] The spanwise grid spacing for the current computations and those of Hansen and Forsythe[3] is 10 nodes per cylinder diameter while the structured mesh for the fully-turbulent solution summarized in the table from Travin *et al.*[2] employed a spanwise resolution of 15 grid points per diameter.

In general, the table shows that there is good agreement between the present DES97 and DDES predictions and the corresponding results from Travin *et al.*[2] and Hansen and Forsythe.[3] The drag coefficient C_d from all of the simulations is on the low end of the measurements summarized by Roshko,[14] that correspond to a higher Reynolds number range ($3.5 \times 10^6 < Re < 8.4 \times 10^6$). Table 1 also shows that the back pressure is slightly more negative for the DDES which is not inconsistent with the slightly higher rms lift that is predicted compared to the DES97 results (and also Travin *et al.*[2] which have the same rms lift as in the current DES97). An additional contributor to the differences in Table 1 is the difference in sampling periods.

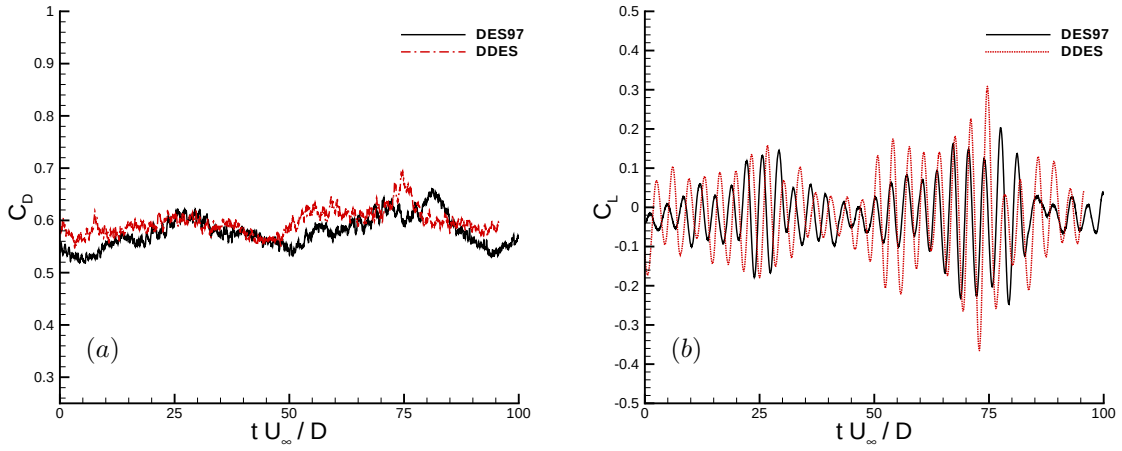

Figure 2. Time history of the drag (in a) and lift (in b) force coefficients, $Re = 1.4 \times 10^5$.

Time histories of the drag and lift coefficients for each model are plotted in Figure 2a and Figure 2b, respectively. Each figure shows comparable behavior for the two models, including the significant modulation in the lift force as also reported in Travin *et al.*[2] and Hansen and Forsythe.[3] These modulations require very long sample periods for convergent statistics, probably longer than those shown in Figure 2, which again contributes to the differences in the statistics summarized in Table 1.

Figure 3 shows the pressure and skin friction coefficients from the two models along with the DES97 predictions of Travin *et al.*[2] and experimental measurements from Roshko[14] and van Nunen[15] for C_p and

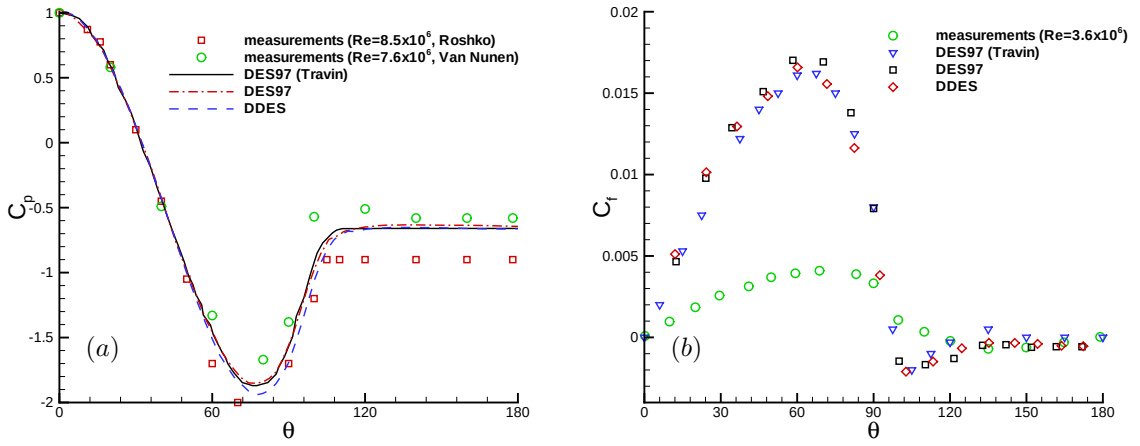

Figure 3. Cylinder pressure coefficient (in a) and skin friction coefficient (in b), $Re = 1.4 \times 10^5$.

Achenbach[21] for C_f. The experimental measurements of the pressure coefficient are at substantially higher Reynolds number (8.4×10^6 in Roshko[14] and 7.6×10^6 in van Nunen[15]) than the computations though the fully turbulent treatment of the solution at $Re = 1.4 \times 10^5$ can be considered a model of the high Reynolds number experiment so long as transition occurs far upstream of separation. Figure 3a shows that both the current DES97 and DDES predictions and the DES97 predictions of Travin *et al.*[2] are in very good agreement and fall within the range of the experiments. While there is generally good agreement between the simulations and experiments in the pressure coefficient in Figure 3a, Figure 3b shows that the skin friction distribution for all of the simulations is far above the experimental measurements prior to separation. The simulation results are consistent with the fully turbulent treatment of the boundary layers while the experiments indicate that the boundary layers were laminar even close to the separation line. Further, the variation in C_f following separation is rather different in the measurements and DES cases shown.

B. DES Predictions at $Re = 8 \times 10^6$

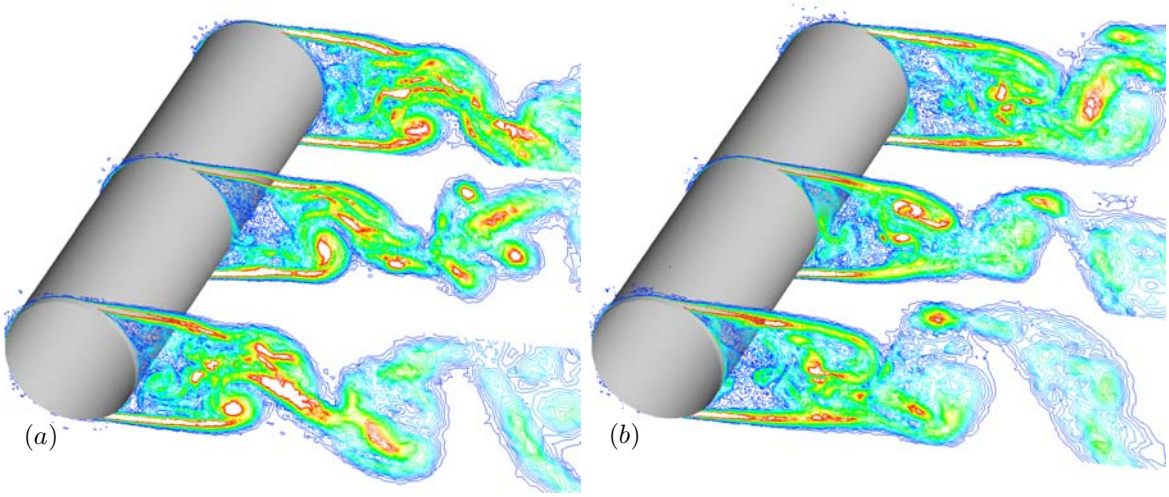

Figure 4. Contours of the instantaneous vorticity from the fine-grid solutions, $Re = 8 \times 10^6$. (a) DES97; (b) DDES.

Contours of the instantaneous vorticity magnitude in three planes along the cylinder span are shown

in Figure 4. The visualizations shown in the figure are from the fine grid DES97 and DDES predictions. Characteristic of a natural DES application in a flow experiencing massive separation, the figure shows that the eddy content in the wake develops rapidly following boundary layer detachment. Importantly, Figure 4 also shows that the three-dimensional structure of the wake resolved in the DDES appears qualitatively similar to that obtained using DES97.

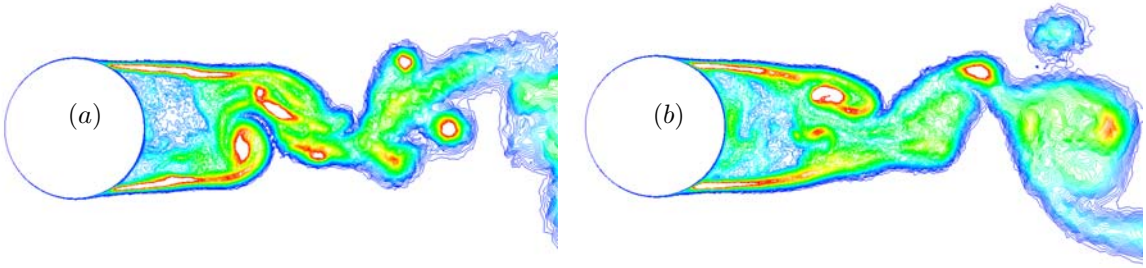

Figure 5. Contours of the instantaneous eddy viscosity ratio from the fine-grid solutions, $Re = 8 \times 10^6$. Contour range is from 0 to $2000\nu_t/\nu$. (a) DES97; (b) DDES.

Contours of the instantaneous eddy viscosity ratio, ν_t/ν in a single spanwise plane along the cylinder are shown in Figure 5. Analogous to Figure 4, the flow structure is comparable between the DES97 prediction in Figure 5a and DDES prediction in Figure 5b. The figure also shows similar ranges in the eddy viscosity levels achieved by the two models. Both Figure 4 and Figure 5 indicate that DDES has not altered the character of the flow structure or turbulence model in the wake relative to the DES97 predictions.

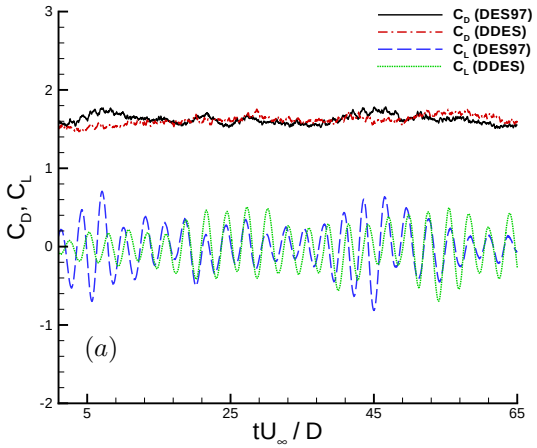

Figure 6. Time history of the drag and lift force coefficients on the medium grid, $Re = 8 \times 10^6$.

Time histories of the drag and lift force coefficients for the medium grid are shown in Figure 6. Analogous to the behavior observed at the lower Reynolds number and shown in Figure 2, there is a noticeable modulation in the lift force at $Re = 8 \times 10^6$ on the medium grid. The averaged drag coefficient, shedding Strouhal number, and separation angle for each of the grids and both the DES97 and DDES models is summarized in Table 2. With the exception of the DDES prediction using the coarsest grid, the averaged properties predicted by the two models are in quite good agreement. In general, the drag coefficient is around 0.4, which agrees well with the value of 0.41 reported in Travin *et al.*[2] from DES97 predictions at $Re = 3 \times 10^6$. With the exception of the coarsest grid, the shedding Strouhal numbers are 0.36-0.37, also close to the value of 0.35 in Travin *et al.*,[2] again at $Re = 3 \times 10^6$. With the exception of the coarsest grid, boundary layer separation occurs at 114°, slightly more aft than the value of 111° in the fully turbulent DES97 prediction at

DES97	C_d	St	θ_{sep}
coarse grid	0.43	0.34	114°
medium grid	0.40	0.36	114°
fine grid	0.37	0.37	114°
DDES	C_d	St	θ_{sep}
coarse grid	0.46	0.33	118°
medium grid	0.40	0.37	114°
fine grid	0.38	0.37	114°

Table 2. Summary of $Re = 8 \times 10^6$ predictions.

3×10^6 in Travin *et al.*[2] As with the discrepancies noted at the lower Reynolds number, the sampling period for the statistics was not uniform (due to computer limitations) and the coarse-grid DDES in the table was sampled $40D/U_\infty$, half as long as the corresponding DES97 result. Further, at the time of submission of this manuscript the fine-grid results for both the DES97 and DDES runs have been sampled for only $20D/U_\infty$.

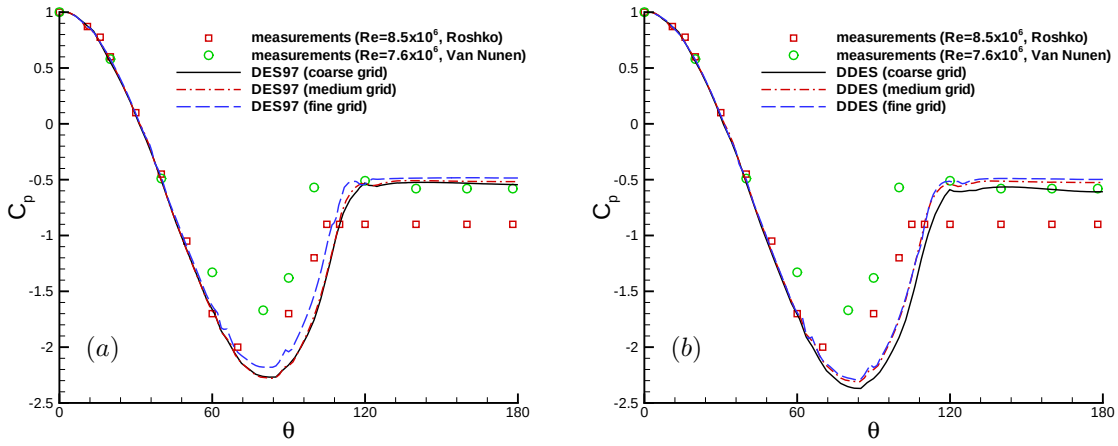

Figure 7. Coefficient of pressure on the cylinder surface, $Re = 8 \times 10^6$. (a) DES97; (b) DDES.

The pressure coefficient for both models and each grid is compared to the experimental measurements of Roshko[14] and van Nunen[15] in Figure 7. The figure shows that there is little sensitivity to the mesh, the differences visible in the figure is likely more an effect of statistical sampling rather than modeling and/or numerical errors. Comparison of the frames shows that the models predict similar pressure distributions, consistent with the close agreement observed in the drag coefficient discussed above. Comparison against Figure 3a for the lower Reynolds number prediction at $Re = 1.4 \times 10^5$ shows the pressure recovery in the aft region is slightly improved at the higher Reynolds number. Further, the pressure minimum in the vicinity of $\theta \approx 85°$ seems clearly deeper than in the experiments.

Properties of the turbulence model are shown in Figure 8. Plotted in the figures are radial profiles of the mean velocity, eddy viscosity ratio, and $\widetilde{d}/d$ at $\theta = 75°$ and $\theta = 90°$. The quantities shown in the figure are DDES predictions for each of the grids. Note that the mean velocities are averaged, the profiles of the eddy viscosity and $\widetilde{d}/d$ are not averaged. Though not shown here, the results from the DES97 cases are virtually identical. For both locations, Figure 8 shows the RANS-LES interface (the location where $\widetilde{d}$ becomes less than d) moves closer to the wall as the grid is refined though for this natural application – thin boundary layers into a region of massive separation – the interface remains well outside of the boundary layer.

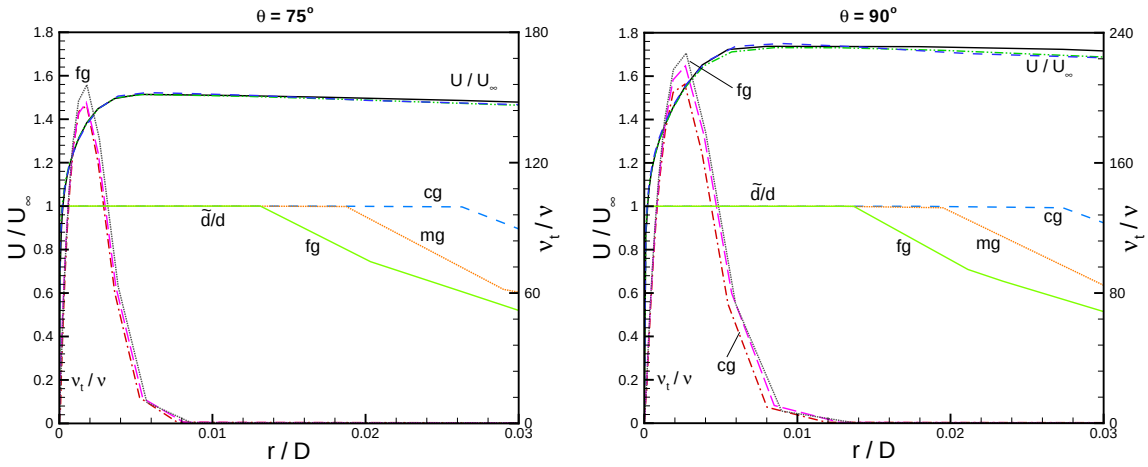

Figure 8. Turbulence model properties and mean velocity from the DDES. (*a*) $\theta = 75°$; (*b*) $\theta = 90°$.

V. Summary

Detached-Eddy Simulation was used to predict the massively separated flow around a circular at Reynolds numbers based on the cylinder diameter and freestream velocity of 1.4×10^5 and 8×10^6. Two versions of the method were applied, the baseline version, DES97, and a new version, DDES, that determines the turbulent length scale using information not only on the wall distance and grid but also the eddy viscosity field.

DES predictions at $Re = 1.40 \times 10^5$ show that there are not significant differences in the statistics obtained using DES97 and DDES and that the simulation results agree well with related studies by Travin *et al.*[2] and Hansen and Forsythe.[3] Flow visualizations show that there the structural features resolved by the baseline version, DES97, and new version, DDES, are also quite similar. Computations at $Re = 8 \times 10^6$ and using three grids yielded similar conclusions as at the lower Reynolds number. The DES97 and DDES predictions are essentially the same for the cylinder flow and in reasonable agreement with experimental measurements of the pressure coefficient.

A. Acknowledgments

The authors gratefully acknowledge the support of the Air Force Office of Scientific Research (Grant FA9550-04-1-0030, Program Officer: Lt Col. Rhett Jefferies and numerous helpful discussions with Dr. Philippe Spalart. The work was performed as part of a DoD Challenge project, on the Aeronautical Systems Center Major Shared Resource Center and the Maui High Performance Computing Center.

References

[1]Spalart, P., Deck, S., Shur, M., Squires, K., Strelets, M. K., and Travin, A., "A New Version of Detached-Eddy Simulation, Resistant to Ambiguous Grid Densities," *Theoretical and Computational Fluid Dynamics*, to appear.

[2]Travin, A., Shur, M., Strelets, M., and Spalart, P., "Detached-eddy simulations past a circular cylinder," *Flow, Turbulence, and Combustion*, Vol. 63, 1999, pp. 293–313.

[3]Hansen, R. and Forsythe, J., "Large and Detached Eddy Simulations of a Circular Cylinder Using Unstructured Grids," Aiaa 2003-0775, 2003.

[4]Spalart, P., Jou, W., Strelets, M., and Allmaras, S., "Comments on the Feasibility of LES for Wings, and on a Hybrid RANS/LES Approach," *First AFOSR International Conference on DNS/LES*, Ruston, Louisiana, 1997.

[5]Squires, K., Forsythe, J., and Spalart, P., "Detached-Eddy Simulation of the separated flow around a forebody cross-section," *Direct and Large Eddy Simulation IV*, Kluwer Academic Press, 2001, pp. 481–500.

[6]Deck, S., Garnier, E., and Buillen, P., "Turbulence modelling applied to space launcher configurations," *Journal of Turbulence*, Vol. 3, 2002.

[7]Forsythe, J., Hoffmann, K., Cummings, R., and Squires, K., "Detached-Eddy Simulation with compressibility corrections applied to a supersonic axisymmetric base flow," Vol. 124, 2002, pp. 911–923.

[8]Morton, S., Steenman, M., Cummings, R., and Forsythe, J., "DES grid resolution issues for vortical flows on a delta wing and an F-18C," Aiaa 2003-1103, 2003.

[9]Forsythe, J. and Woodson, S., "Unsteady CFD Calculations of Abrupt Wing Stall Using Detached-Eddy Simulation," Aiaa 2003-0594, Jan. 2003.

[10]Viswanathan, A., Klismith, K., Forsythe, J., and Squires, K., "Detached-Eddy Simulation Around a Rotating Forebody," Aiaa 2003-0263, Jan. 2003.

[11]Forsythe, J., Squires, K., Wurtzler, K., and Spalart, P., "Detached-Eddy Simulation of the F-15E at High Alpha," *Journal of Aircraft*, Vol. 41, No. 2, 2004, pp. 193–200.

[12]Spalart, P. and Allmaras, S., "A One-Equation Turbulence Model for Aerodynamic Flows," *La Recherche Aerospatiale*, Vol. 1, 1994, pp. 5–21.

[13]Menter, F., Kuntz, M., and Bender, R., "A Scale-Adaptive Simulation Model for Turbulent Flow Predictions," Aiaa 2003-0767, 2003.

[14]Roshko, A., "Experiments on the Flow past a Circular Cylinder at Very High Reynolds Number," *Journal of Fluid Mechanics*, Vol. 10, No. 3, 1961, pp. 345–356.

[15]Nunen, J. V., "Pressure and Forces on a Circular Cylinder in a Cross flow at High Reynolds Numbers," *Flow Induced Structural Vibrations*, Springer-Verlag, Berlin, 1974, pp. 748–754.

[16]Shur, M., Spalart, P., Strelets, M., and Travin, A., "Detached-Eddy Simulation of an Airfoil at High Angle of Attack," *4th International Symposium of Engineering Turbulence Modeling and Measurements*, Corsica, May 1999.

[17]Strang, W., Tomaro, R., and Grismer, M., "The Defining Methods of Cobalt$_{60}$: a Parallel, Implicit, Unstructured Euler/Navier-Stokes Flow Solver," Aiaa paper 99–0786, Jan. 1999.

[18]Gottlieb, J. and Groth, C., "Assessment of Riemann Solvers for Unsteady One-Dimensional Inviscid Flows of Perfect Gases," *Journal of Computational Physics*, Vol. 78, 1988, pp. 437–458.

[19]G. Karypis, K. S. and Kumar, V., *ParMETIS: Parallel Graph Partitioning and Sparse Matrix Ordering Library Version 1.0*, University of Minnesota, Department of Computer Science, Minneapolis, MN, 1997.

[20]Pirzadeh, S., "Three-dimensional Unstructured Viscous Grids by the Advancing Layers Method," *AIAA Journal*, Vol. 34, 1996, pp. 43–49.

[21]Achenbach, E., "Distribution of local pressure and skin friction around a circular cylinder in cross-flow up to Re = 5 x 10^6," *Journal of Fluid Mechanics*, Vol. 34, No. 4, 1968, pp. 625–639.